

Spinning superfluid helium-4 nanodroplets

Francesco Ancilotto,^{1,2} Manuel Barranco,^{3,4,5} and Martí Pi^{3,4}

¹*Dipartimento di Fisica e Astronomia “Galileo Galilei” and CNISM,
Università di Padova, via Marzolo 8, 35122 Padova, Italy*

²*CNR-IOM Democritos, via Bonomea, 265 - 34136 Trieste, Italy*

³*Departament FQA, Facultat de Física, Universitat de Barcelona. Diagonal 645, 08028 Barcelona, Spain*

⁴*Institute of Nanoscience and Nanotechnology (IN2UB), Universitat de Barcelona, Barcelona, Spain.*

⁵*Université Toulouse 3 and CNRS, Laboratoire des Collisions, Agrégats et Réactivité,
IRSAMC, 118 route de Narbonne, F-31062 Toulouse Cedex 09, France*

(Dated: December 14, 2024)

We have studied spinning superfluid ^4He nanodroplets at zero temperature using Density Functional theory. Due to the irrotational character of the superfluid flow, the shapes of the spinning nanodroplets are very different from those of a viscous normal fluid drop in steady rotation. We show that when vortices are nucleated inside the superfluid droplets, their morphology is in good agreement with experiments. The presence of vortex arrays confers to the superfluid droplets the rigid-body behavior of a normal fluid in steady rotation, and this is the ultimate reason of the surprising good agreement between recent experiments and the classical models used for their description.

When a drop made of a normal liquid rotates, centrifugal forces push the liquid away from the axis of rotation producing deformations which change its spherical appearance at rest into an oblate, axisymmetric shape. If the drop spins fast enough, it may eventually distort into a two-lobed, peanut-shaped form before undergoing fission when it is no longer able to sustain the strain due to its own rotational motion.

Hydrodynamical models aiming at describing rotating fluid drops have been successfully applied to systems that range from atomic nuclei to celestial objects. Most theoretical models assume the liquid to be incompressible and viscous so that drops eventually reach a steady state in which they rotate as if they were rigid bodies. There exists a vast literature on the subject, see e.g. Refs. [1–9] and references therein.

Using wax samples under diamagnetic levitation, the theoretical shapes of rotating drops were reproduced experimentally [8]. Experiments using water drops [6] and drops made of a mixture of tertbutanol and water [9] have also been carried out. These studies are especially interesting because they provide direct experimental validation of numerical models used to calculate equilibrium shapes of spinning drops made of classical fluids. With increasing angular momentum, the shapes of the wax samples in Ref. [8] progress from spheres (not rotating) to oblate-like shapes, to tri-axial shapes (three unequal axes), and finally to two-lobed (dumbbell) shapes. In oblate-like and tri-axial shapes, the shortest axis coincides with the axis of rotation. In two-lobed shapes the axis of rotation is perpendicular to the line joining the centers of the two lobes.

With the experimental realization of superfluid helium drops using cryogenic free-jet gas expansions [10], attention has been focused recently on the shapes of superfluid drops. It is commonly accepted that helium drops

created in the normal, non-superfluid phase, may acquire angular momentum during the passage of the fluid through the nozzle of the experimental apparatus [11]. Vorticity, defined in hydrodynamics as $\nabla \times \mathbf{v}$ [12], where \mathbf{v} is the velocity field of the fluid, is distributed inside the drop in the normal phase. It equals 2ω for a rotating rigid body, or for a viscous fluid in steady rotation, ω being the angular velocity about the rotation axis.

During the expansion process the helium drops cool down to about 0.4 K temperature (T); at this temperature, the helium is superfluid and the normal fluid fraction is negligible. The spinning superfluid drops retain a large yet unknown fraction of the angular momentum deposited in them when they are still in the normal phase. Since the superfluid flow is irrotational, $\nabla \times \mathbf{v} = 0$, the vorticity remaining in the drops is concentrated in the cores of the quantized vortices nucleated in the drop interior [13] and in capillary waves [14]. This is the mechanism by which angular momentum is conserved in an isolated helium drop undergoing a normal to superfluid state transition.

Superfluid ^4He drops in fast rotation have been studied by coherent x-ray scattering [15]. The shapes of the drops observed were consistent with those of axisymmetric oblate pseudo-spheroids with large aspect ratio, defined as the ratio of the long half-axis length to the short half-axis length along the rotational axis. Interestingly, the existence of vortex arrays inside a number of drops was established by the appearance of Bragg patterns from Xe clusters trapped in the vortex cores [15]. It is worth stressing that doping the drops was instrumental for detecting the presence of vortices, the extremely small size of the vortex cores preventing their direct detection. At variance, the shapes of the drops could be instead inferred in the absence of doping.

While normal fluid drops change their shape as ro-

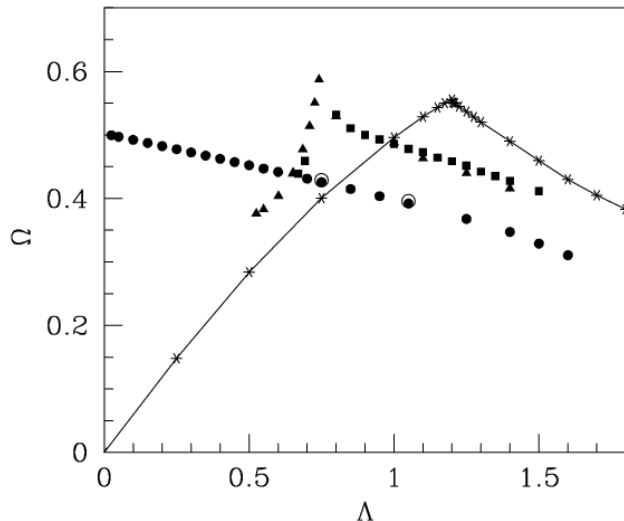


FIG. 1: Rescaled angular velocity Ω vs. rescaled angular momentum Λ . Triangles: 3-vortex configurations; squares: 4-vortex configurations; dots: vortex-free configurations. The starred symbols connected by a solid line are the classical rotating drop results of Ref. [7].

tation becomes faster to resemble a “peanut” (two-lobe shape) or a “blood cell” [1, 3, 6], no evidence of such shape shifting was seen in the experiments of Ref.15. Density Functional Theory (DFT) calculations carried out for droplets containing 15000 ^4He atoms and up to $n_v = 9$ vortices, confirmed the above scenario [16, 17], the comparison with the experimental measurements being facilitated by using suitably rescaled units to characterize the droplet shapes (see below), which showed indeed remarkable similarities with the experimental drops.

Some helium droplets displaying prolate shapes have also been detected [11] using small-angle x-ray diffraction experiments [11, 15, 18]. More recently, coherent diffractive imaging experiments of rotating ^4He drops using extreme ultraviolet pulses in conjunction with wide-angle x-ray diffraction have allowed to identify, in addition to oblate shapes, a large number of prolate shapes and even two-lobed drops [19, 20].

Comparison of the experimental droplet shapes with those predicted by numerical calculations for normal liquid rotating drops [8] showed a good agreement. It was thus concluded that helium drops formed in the free jet expansion surprisingly follow closely the sequence of shapes characteristic of normal fluid drops.

The most natural question arises, i.e. why spinning superfluid ^4He drops, whose hydrodynamical hallmark is irrotational flow, behave instead as rotational normal liquid drops. The answer, as we will show in the following, is the presence of vortex arrays in the helium drops which make them behave in a manner apparently similar to classical rotating fluids.

The similarity between rotating superfluid ^4He and the rigid-body rotation of a viscous liquid has been proven long ago for bulk ^4He in a rotating bucket: in spite of its irrotational flow, ^4He develops a meniscus just like a rotating normal fluid, instead of remaining at rest with a flat liquid-vapor interface [21]. This apparently contradictory behavior has been explained by the nucleation of quantized vortices which carry most of the angular momentum of the rotating fluid. The larger the number of vortices, the closer the rotation to that of a rigid body, vorticity eventually reaching 2ω for large angular velocities [13, 22].

We have used Density Functional Theory to describe superfluid helium droplets [25]. Within DFT, the total energy E of a $^4\text{He}_N$ droplet at $T = 0$ is written as a functional of a complex effective wave function $\Psi(\mathbf{r})$ related to its atomic density by $\rho(\mathbf{r}) = |\Psi(\mathbf{r})|^2$

$$E[\rho] = \frac{\hbar^2}{2m_{\text{He}}} \int d\mathbf{r} |\nabla\Psi|^2 + \int d\mathbf{r} \mathcal{E}_c[\rho] \quad (1)$$

The first term is the kinetic energy of a fictitious system of non-interacting particles (with mass m_{He}) and the second term is the correlation energy, for which we have taken that proposed in Ref. [23]. This functional is finite-range and includes non-local effects. Both aspects are needed to describe quantitatively the response of the liquid at the \AA -scale.

The droplet equilibrium configuration is obtained by solving the Euler-Lagrange (EL) equation arising from functional variation of Eq. (1), i.e.

$$\left\{ -\frac{\hbar^2}{2m_{\text{He}}} \nabla^2 + \frac{\delta\mathcal{E}_c}{\delta\rho} \right\} \Psi(\mathbf{r}) \equiv \mathcal{H}[\rho] \Psi(\mathbf{r}) = \mu_4 \Psi(\mathbf{r}) \quad (2)$$

where μ_4 is the ^4He chemical potential. Unless explicitly stated, the number of helium atoms in the studied droplets is $N = 1500$.

To investigate non-zero angular momentum configurations in the spinning droplet it is convenient to move to the fixed-droplet frame of reference (corotating frame) by imposing, through the use of a Lagrange multiplier ω , a fixed value for the total angular momentum $\langle L_z \rangle$, i.e. we look for solutions of the equation

$$\{ \mathcal{H}[\rho] - \omega \hbar \hat{L}_z \} \Psi(\mathbf{r}) = \mu_4 \Psi(\mathbf{r}) \quad (3)$$

where \hat{L}_z is the dimensionless angular momentum operator. The results presented in this work have been obtained using the 4He-DFT BCN-TLS computing package [24]. Details on how Eqs. (2) and (3) are solved can be found in Ref. [25] and references therein. We work in 3D cartesian coordinates and no symmetry is imposed to the droplet.

As in previous studies [5, 7, 11], we use here rescaled units for angular momentum, Λ , and angular velocity, Ω . This allows to compare our results, which are obtained

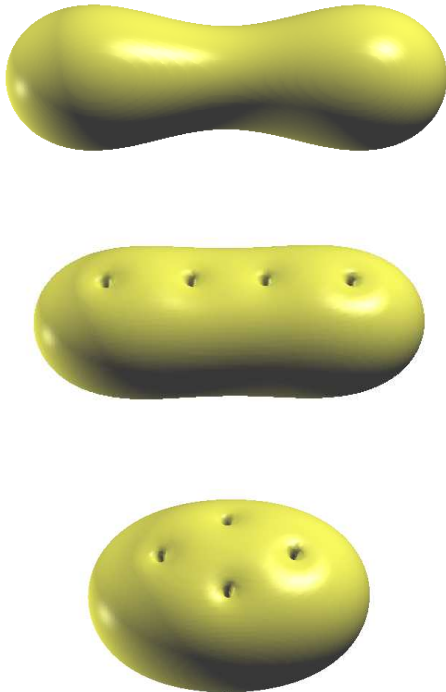


FIG. 2: Prolate ${}^4\text{He}_{1500}$ droplet shapes represented by their sharp density surfaces. Top: Vortex-free configuration with $\Lambda = 1.5$; Middle: 4-vortex linear configuration with $\Lambda = 1.5$; Bottom: 4-vortex cross configuration with $\Lambda = 0.9$.

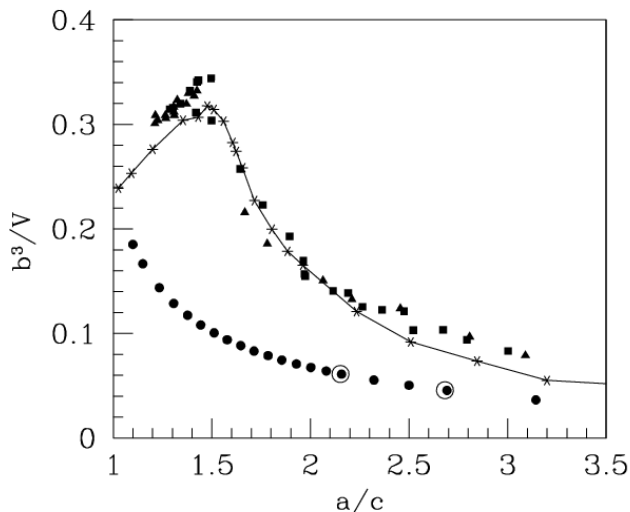


FIG. 3: Aspect-ratio b^3/V vs. a/c curve. Triangles: 3-vortex configurations; squares: 4-vortex configurations; dots: vortex-free configurations. Big empty dots show values for the ${}^4\text{He}_{5000}$ droplet. The starred symbols connected by a solid line correspond to the classical result from Ref. [8].

for droplets made of $O(10^3)$ atoms, with experimental results on large drops, made of $10^8 - 10^{11}$ atoms. Such units are defined as [26]

$$\Omega \equiv \sqrt{\frac{m_{\text{He}} \rho_0 R^3}{8\gamma}} \omega \quad (4)$$

$$\Lambda \equiv \frac{\hbar}{\sqrt{8\gamma R^7 m_{\text{He}} \rho_0}} L_z$$

In the above expressions, $\gamma = 0.274 \text{ K } \text{\AA}^{-2}$ and $\rho_0 = 0.0218 \text{ \AA}^{-3}$ are the surface tension and liquid atom density at $T = P = 0$, R is the sharp radius of the spherical helium droplet when $L_z = 0$, and r_0 is the bulk radius defined such that $4\pi r_0^3 \rho_0 / 3 = 1$. For liquid ${}^4\text{He}$ one has $R = r_0 N^{1/3}$ with $r_0 = 2.22 \text{ \AA}$. Moreover, $\hbar^2 / m_{\text{He}} = 12.12 \text{ K } \text{\AA}^2$. Liquid helium is fairly incompressible and hence the volume of any deformed configurations can be safely identified with $V = 4\pi R^3 / 3$.

We have employed two different strategies to solve Eq. (3), i.e. we either (i) fix ω and find the associated stationary configuration, which will be characterized by some value of the angular momentum L_z depending upon the chosen value of ω , or (ii) solve Eq. (3) by imposing a given value for L_z and iteratively find the associated value of ω . Classically, the fixed omega calculations correspond to forced rotation conditions while the fixed L_z calculations correspond to torque free drops with an initial rotation. As shown in the following, (i) allows to find the stable oblate configurations of the rotating droplet [16], while (ii) allows to find instead the prolate configurations [3].

The $\Omega(\Lambda)$ relationship for normal fluid drops in steady rotation is plotted with a solid line in Fig. 1 [7]. Configurations with $\Lambda \lesssim 1.2$ have oblate axisymmetric shapes, and configurations with larger Λ values have prolate triaxial or two-lobed shapes [3–5, 7]; the classical bifurcation point is at $(\Lambda, \Omega) \sim (1.2, 0.56)$ [26].

As shown also in Fig. 1, the calculated $\Omega(\Lambda)$ relation for a superfluid droplet (filled dots) is very different. In this case, only prolate triaxial configurations may exist since axisymmetric oblate configurations are quantum mechanically forbidden [27]. One such prolate configuration corresponding to $\Lambda = 1.5$ is shown in the top panel of Fig. 2. Let us mention that the two empty circles in Fig. 1 have been calculated using a $N = 5000$ atoms droplet (see also Fig. 3). The purpose of these calculations has been to check explicitly the scaling of the results with the number of atoms in the droplet.

To allow for a sensible comparison with the experimental and classical results, we have determined the aspect ratio of the superfluid droplets. For any stationary configuration obtained solving Eq. (3), a sharp density surface is defined by calculating the locus at which the helium density equals $\rho_0/2$; for a spherical distribution this corresponds to a sphere of radius R . In the case of deformed droplets, three lengths are introduced representing the distances from the droplet center of mass

(COM) to the sharp surface along the rotation axis (c); the largest distance from the COM to the sharp surface along an axis perpendicular to the rotation axis (a); and a third length (b) corresponding to the distance of the COM to the sharp surface in the direction perpendicular to the other two. For an axisymmetric droplet $a = b \neq c$, whereas $a \neq b \neq c$ in the case of triaxial, prolate shapes.

Figure 3 displays b^3/V vs. the ratio a/c ; when $a/c = 1$, $b^3/V = R^3/V = 3/(4\pi)$. The solid line shows the classical model result and the filled dots (lower curve) correspond to superfluid droplets. As for the $\Omega(\Lambda)$ curve in Fig. 1, it may be seen that the rotational normal fluid and the irrotational superfluid results are very different.

Finally, we have calculated the equilibrium shapes of rotating ^4He droplets hosting vortices. It is worth recalling that oblate-like configurations can only store angular momentum by nucleating a number of vortices in their interior, in the form of a vortex array that reduces the $D_{\infty h}$ symmetry of the axisymmetric vortex-free droplet to, e.g., a D_{nh} symmetry if n vortices are evenly distributed in a ring around the droplet center. Examples of oblate-like configurations hosting a different number of vortices have been presented in Ref. [16].

Helium-4 droplets hosting quantized vortices are addressed using the “imprinting” procedure [16, 25] by which n_v vortex lines parallel to the z axis are initially created, starting the energy minimization from the effective wave function

$$\Psi_0(\mathbf{r}) = \rho_0^{1/2}(\mathbf{r}) \prod_{j=1}^{n_v} \left[\frac{(x - x_j) + i(y - y_j)}{\sqrt{(x - x_j)^2 + (y - y_j)^2}} \right] \quad (5)$$

where (x_j, y_j) is the initial position of the linear j -th vortex core with respect to the z -axis of the droplet, and $\rho_0(\mathbf{r})$ is a vortex-free density. These vortex positions are guessed and during the functional minimization of the total energy, both the vortex positions and droplet density are allowed to change to provide at convergence the lowest energy configuration for the chosen value of ω or L_z .

The middle panel in Fig. 2 displays one of such prolate configuration hosting $n_v = 4$ vortices for $\Lambda = 1.5$. This n_v is the largest number of vortices the $N = 1500$ atoms droplet may accommodate. Depending upon the value of Λ , the vortex cores can be either arranged in a cross-like configuration (energetically favored for lower values of Λ) or aligned along the largest droplet axis (at higher Λ values). The bottom panel in Fig. 2 displays a prolate droplet hosting four vortices in a cross configuration for $\Lambda = 0.9$.

We display in Fig. 1 the $\Omega(\Lambda)$ relationship for the rotating droplets hosting $n_v = 3$ and 4 vortices (squares and triangles, respectively). Interestingly, the resulting curve shows a resemblance with the classical model predictions [8]. The difference between the irrotational superfluid and rotational normal flow stability curves in

Fig. 1 indicates how different is the way in which angular momentum is stored in the two cases.

The b^3/V vs. a/c curve in the presence of vortices displays a rising branch in the left part of the aspect-ratio curve of Fig. 3 corresponding to oblate-like configurations. Remarkably, the oblate-like part of that curve stops close to the value $a/c = 1.5$, which is the classical stability limit for axisymmetric configurations [1]. Nearly from this a/c value on, the stationary configurations have prolate shapes.

Figure 3 contains the key results of the present study, that we summarize as follows:

- For a given Λ value, a description of superfluid helium droplets in terms of vortex-free, irrotational flow drops yields droplet shapes that are much different from the classical model ones and thus from the experiment [19, 20]. It is worth stressing that, while the drop morphology is now an available experimental information [19, 20], its angular velocity and the angular momentum are not.
- The presence of vortices drastically modify the sequence of permitted droplet shapes, in particular allowing the appearance of stable axisymmetric (oblate) shapes. One should recall that “any container of superfluid helium, treated in conventional fashion, will be permeated *ab initio* by numerous quantized vortices stabilized by surface pinning” [28]. Given the way they are produced, there is no reason why ^4He drops, viewed as self-sustained containers, should not host a number of vortices.

- Our calculations show that when the number of vortices in the droplet is close to its maximum possible (four in the case of the small droplet used in our DFT calculations), the aspect-ratio b^3/V vs. c/a curve agrees with that obtained using the classical rotating droplet model. Some differences are expected to show up between both approaches, as drops are considered incompressible and the existence of any surface width is neglected in classical models, whereas within DFT liquid compressibility and surface width are taken into account.

The rotating bucket experiment tells us that the presence of vortex arrays confers to rotating superfluid helium samples the appearance of a rotating rigid body; we have shown here that the same happens for a rotating ^4He droplet. From the global good agreement between experiments and classical models of rotation regarding the droplet morphology [19, 20], we conclude that these droplets must host quantized vortices whose presence could be determined after doping them [15].

We notice that at high values of the ratio a/c (i.e. high values of the angular momentum) the calculated shapes start deviating from the classical results. We attribute this to the fact that classical drops with high Λ 's acquire a peanut-like shape, whereas when vortices are present, a more pill-like shape is instead realized, where the depression in the center of the elongated droplet is either absent or less pronounced than in the classical case (compare the

upper and middle panels in Fig. 2).

Let us mention that deformed vortex-free spinning helium droplets are also stable objects in which the angular momentum has been stored as giant capillary waves. The vortex-free droplets are stable up to much larger values of a/c than those hosting vortices. In particular, we have found stable configurations for c/a as large as 4.5, whereas the largest a/c values displayed in Fig. 3 for the droplets hosting vortices correspond to their actual stability limit.

We would like to conclude indicating that, although these vortex-free droplets are likely a fairly small fraction of the –already small– fraction of deformed drops identified in the experiments (the majority of the imaged ^4He drops in Ref. [20] are spherical, only a 10% showed diffraction patterns corresponding to deformed shapes), the DFT results in Fig. 3 might help locate these configurations which so far apparently have escaped direct measure. According to the figure, the region around $a/c \sim 1.5$ seems to be to most adequate for their search as there the b^3/V value is very different from that of vortical droplets.

We thank Jordi Boronat, Andrey Vilesov, Sam Butler, and Bruno Langbehn for useful discussions and exchanges. We are most indebted to Sam Butler for providing us with the results of the classical model calculations. This work has been performed under Grants No 2014SGR401 from Generalitat de Catalunya and FIS2014-52285-C2-1-P from DGI (Spain). MB thanks the Université Fédérale Toulouse Midi-Pyrénées for financial support throughout the “Chaires d’Attractivité 2014” Programme IMDYNHE.

-
- [1] S. Chandrasekhar, *Prog. R. Soc. Lond. A* **286**, 1 (1965).
 [2] S. Cohen, R. Plasil, and W.J. Swiatecki, *Ann. Phys.* **82**, 557 (1974).
 [3] R.A. Brown and L.E. Scriven, *Proc. R. Soc. Lond. A* **371**, 331 (1980).
 [4] R.A. Brown and L.E. Scriven, *Phys. Rev. Lett.* **45**, 180 (1980).
 [5] C.-J. Heine, *IMA J. Num. Anal.* **26**, 723 (2006)
 [6] R.J.A. Hill and L. Eaves, *Phys. Rev. Lett* **101**, 234501 (2008).
 [7] S.L. Butler, M.R. Stauffer, G. Sinha, A. Lilly, and R.J. Spiteri, *J. Fluid Mech.* **667**, 358 (2011).
 [8] K.A. Baldwin, S.L. Butler, and R.J.A. Hill, *Sci. Rep.* **5**, 7660 (2015).
 [9] L. Liao and R.J.A. Hill, *Phys. Rev. Lett* **110**, 114501 (2017).
 [10] J.P. Toennies and A.F. Vilesov, *Angew. Chem. Phys.* **43**, 2622 (2004).
 [11] C. Bernando, R.M.P. Tanyag, C. Jones, C. Bacellar, M. Bucher, K.R. Ferguson, D. Rupp, M. P. Ziemkiewicz, L.F. Gomez, A.S. Chatterley, T. Gorkhover, M. Müller, J. Bozek, S. Carron, J. Kwok, S.L. Butler, Thomas Möller, Ch. Bostedt, O. Gessner, and A.F. Vilesov, *Phys. Rev. B* **95**, 064510 (2017).
 [12] E. Guyon, J.-P. Hulin, L. Petit, and C.D. Matescu, *Physical Hydrodynamics*, 2nd. ed., Oxford University Press, Oxford, U.K., 2015.
 [13] R.J. Donnelly, *Quantized vortices in helium II*, Cambridge Studies in Low Temperature Physics, Cambridge University Press, Cambridge, U.K. 1991, Vol. 3.
 [14] D.L. Whitaker, M.A. Weilert, C.L. Vicente, H.J. Maris, and G.M. Seidel, *J. Low Temp. Phys.* **110**, 173 (1998).
 [15] L.F. Gomez, K.R. Ferguson, J.P. Cryan, C. Bacellar, R.M.P. Tanyag, C. Jones, S. Schorb, D. Anielski, A. Belkacem, C. Bernando, R. Boll, J. Bozek, S. Carron, G. Chen, T. Delmas, L. Englert, S.W. Epp, B. Erk, L. Foucar, R. Hartmann, A. Hexemer, M. Huth, J. Kwok, S.R. Leone, J.H. S. Ma, F.R. N. C. Maia, E. Malmerberg, S. Marchesini, D.M. Neumark, B. Poon, J. Prell, D. Rolles, B. Rudek, A. Rudenko, M. Seifrid, K.R. Siefermann, F.P. Sturm, M. Swiggers, J. Ullrich, F. Weise, P. Zwart, C. Bostedt, O. Gessner, and A.F. Vilesov, *Science* **345**, 906 (2014).
 [16] F. Ancilotto, M. Pi and M. Barranco, *Phys. Rev. B* **91**, 100503(R) (2015).
 [17] F. Coppens, F. Ancilotto, M. Barranco, N. Halberstadt, and M. Pi, *Phys. Chem. Chem. Phys.* **19**, 24805 (2017).
 [18] C.F. Jones, C. Bernando, R.M.P. Tanyag, K.R. Ferguson, C. Bacellar, L. Gomez, D. Anielski, A. Belkacem, R. Boll, J. Bozek, S. Carron, J. Cryan, L. Englert, S.W. Epp, B. Erk, R. Hartmann, L. Foucar, D.M. Neumark, D. Rolles, B. Rudek, A. Rudenko, K.R. Siefermann, F.P. Sturm, J. Ullrich, F. Weise, Ch. Bostedt, O. Gessner, and A.F. Vilesov *Phys. Rev. B* **93**, 180510(R) (2016).
 [19] D. Rupp, N. Monserud, B. Langbehn, M. Sauppe, J. Zimmermann, Y. Ovcharenko, T. Möller, F. Frassetto, L. Polletto, A. Trabattoni, F. Calegari, M. Nisoli, K. Sander, C. Peltz, M. J. J. Vrakking, T. Fennel, and A. Rouzee, *Nature Commun.* **8**, 493 (2017).
 [20] B. Langbehn, Y. Ovcharenko, D. Rupp, K. Sander, C. Peltz, A. Clark, R. Cucini, P. Finetti, M. Di Fraia, D. Iablonskyi, A.C. LaForge, V. Oliver Álvared de Lara, O. Plekan, P. Piseri, T. Nishiyama, C. Calegari, K.C. Prince, K. Ueda, F. Stienkemeier, T. Fennel, and T. Möller, contribution to the Quantum Fluid Cluster Workshop, Obergürgl, Austria, June 6-9 (2017), <https://www.uibk.ac.at/congress/qfc2017>
 [21] D.V. Osborne, *Proc. Phys. Soc. A* **63** 909 (1950).
 [22] L. Pitaevskii and S. Stringari, *Bose-Einstein Condensation and Superfluidity*, International Series of Monographs on Physics vol. 164 Oxford University Press, 2016.
 [23] F. Ancilotto, M. Barranco, F. Caupin, R. Mayol, and M. Pi, *Phys. Rev. B* **72**, 214522 (2005).
 [24] 4He-DFT BCN-TLS: A Computer Package for Simulating Structural Properties and Dynamics of Doped Liquid Helium-4 Systems. M. Pi, F. Ancilotto, F. Coppens, N. Halberstadt, A. Hernando, A. Leal, D. Mateo, R. Mayol, and M. Barranco, <https://github.com/bcntls2016/>
 [25] F. Ancilotto, M. Barranco, F. Coppens, J. Eloranta, N. Halberstadt, A. Hernando, D. Mateo, and M. Pi, *Int. Rev. Phys. Chem.* **36**, 621 (2017).
 [26] We use the Λ definition of Refs. [5, 7, 11] that is four times larger than that of Refs. [3, 4].
 [27] F. Villars, *Ann. Rev. Nucl. Sci.* **7**, 185 (1957).
 [28] D.D. Awschalom and K.W. Schwarz, *Phys. Rev. Lett.* **52**, 49 (1984).